# Superconducting Properties of Nanosized Molybdenum Sulphide (MoS<sub>2</sub>) Added Bi<sub>1.6</sub>Pb<sub>0.4</sub>Sr<sub>2</sub>CaCu<sub>2</sub>O<sub>8</sub> Superconductor

#### Masnita Mat Jusoh1\* and Roslan Abd Shukor2

<sup>1</sup>Centre of Foundation Studies, Universiti Teknologi MARA, Cawangan Selangor, Kampus Dengkil, 43800 Dengkil, Selangor, Malaysia

<sup>2</sup>Department of Applied Physics, Universiti Kebangsaan Malaysia, 43600 Bangi, Selangor, Malaysia \*Corresponding author (e-mail: masnita@uitm.edu.my)

The bismuth-based high temperature with composition  $Bi_{1.6}Pb_{0.4}Sr_2CaCu_2O_8$  (MoS<sub>2</sub>)<sub>x</sub> (Bi-2212) has been prepared using the solid-state reaction process, and the value of x = 1 to 5 wt. %. The size of the MoS<sub>2</sub> was 90 nanometers. The samples were characterized using the four-point probe electrical resistance measurements, AC susceptibility, X-ray diffraction (XRD) and field emission scanning electron microscopy (FESEM). The addition of nanosized MoS<sub>2</sub> showed no changes in the orthorhombic structure and microstructure. The non-added samples recorded the highest transition temperature ( $T_{c \text{ onset}} = 85 \text{ K}$ ). All samples exhibited superconducting properties except for higher concentrations of MoS<sub>2</sub>. Sample with x = 1 wt. % showed the highest peak transition ( $T_p$ ) of the imaginary part of the AC susceptibility. The critical current density at  $T_p$  was between 20.8 and 31.3 A cm<sup>-2</sup>. These findings suggest that adding low levels of MoS<sub>2</sub> improved performance in the superconducting properties while maintaining the structural integrity of the crystal lattice.

Keywords: AC susceptibility; molybdenum sulfide; microstructure; X-ray diffraction

Received: April 2025; Accepted: August 2025

Numerous studies have been conducted to investigate the superconducting properties of high-temperature superconductors. Among these, cuprates stand out as promising candidates for advanced applications due to their high critical temperature  $(T_c)$  and critical magnetic field [1]. The bismuth strontium calcium copper oxide (BSCCO) system, a member of the cuprate family, includes three distinct superconducting phases with the general formula  $Bi_2Sr_2Ca_{n-1}Cu_nO_y$  (where *n* represents the number of CuO<sub>2</sub> layers per unit cell). These phases are Bi<sub>2</sub>Sr<sub>2</sub>Ca<sub>2</sub>Cu<sub>3</sub>O<sub>10</sub> (Bi-2223), Bi<sub>2</sub>Sr<sub>2</sub>Ca<sub>1</sub>Cu<sub>2</sub>O<sub>8</sub> (Bi-2212), and Bi<sub>2</sub>Sr<sub>2</sub>CuO<sub>6</sub> (Bi-2201) [2].

Although BSCCO ceramics exhibit advantages such as high critical temperature and magnetic field-carrying capacity, they also have limitations, including weak links, high anisotropy, and short coherence lengths, which hinder their technological applications [3,4]. Due to weak coupling between BiO layers in the BSCCO system, substituting Bi3+ with other oxides is necessary to enhance their properties [5]. To improve the critical current density  $(J_c)$ , substitution or doping can introduce defects into the crystalline structure, thereby reducing flux creep [6]. However, depending on the characteristics of added or substituted elements, superconducting properties may be either enhanced or destroyed, for example adding TiO decreased the  $J_c$  of a bismuth-based superconductor system [7].

Extensive research has examined the chemical substitution or addition of both magnetic and nonmagnetic impurities to Bi-2212 superconductors to improve their superconducting properties and formation process [5, 8, 9]. Previous studies report that Al doping in Bi-2212 enhances flux pinning forces [10], while other substitutions also improve  $J_c$  [6]. Metal oxides are the most common choice for substitution and doping in high-temperature superconductors. More recently, however, sulfide additions have attracted attention. For example, the sulfide substitution in the YBa<sub>2</sub>Cu<sub>3</sub>O<sub>7-8</sub> (YBCO) system was found to be less detrimental to T<sub>c</sub> compared to metal oxide substitution [11]. Another study also demonstrated that PbS doping reduced voids in the YBCO microstructure and improved grain boundary effects, resulting in higher critical current densities [12]. In addition, adding nanoparticles will possibly improve intergrain connectivity due to their tiny size compared to micro-sized elements [13].

Further research suggests that sulfides can stabilize the Bi-2212 phase and enhance the superconducting transition temperature [14]. The addition of Cr<sub>2</sub>S<sub>3</sub> was found to reduce grain size [15], while CuS nanoparticles in the Bi-2223 system acted as strong pinning centers, thereby improving flux pinning capacity and transport properties [16]. Substituting PbO is also known to increase the volume fraction of the Bi-2223 phase [17].

Building upon these findings, the present work investigates the effect of MoS<sub>2</sub> doping on the superconducting properties of the Bi-2212 phase. With a melting point of 1185°C [18], MoS<sub>2</sub> is unlikely to melt within the system, as this temperature exceeds the Bi-2212 formation temperature (800–820°C). The study presents results from X-ray diffraction, scanning electron microscopy, electrical resistance, and AC susceptibility measurements.

#### **EXPERIMENTAL**

Bi<sub>2</sub>Sr<sub>2</sub>CaCu<sub>2</sub>O<sub>8</sub> samples were synthesized using high-purity powders (≥99.9%) of Bi<sub>2</sub>O<sub>3</sub>, PbO, CaO, and CuO (all obtained from Sigma Aldrich), along with Sr<sub>2</sub>CO<sub>3</sub> (98.5%, GPR from BDH Laboratory Supplies) via the solid-state reaction method. The powders were thoroughly ground and heated in air at 800°C for 24 h with multiple intermittent grindings. The resulting powders were ground again and mixed with 90 nanometer-sized MoS<sub>2</sub>. The initial compositions were Bi<sub>2</sub>Sr<sub>2</sub>CaCu<sub>2</sub>O<sub>8</sub>(MoS<sub>2</sub>)<sub>x</sub>, where x was 0, 1.0, 2.0, 3.0, and 5.0 wt.%. The powders were then pressed into pellets with a diameter of 12.5 mm and a thickness of 2 mm, followed by heating at 820°C for 24 h. The sintering process was conducted in an air atmosphere and furnace cooled down at a rate of 2°C/minute.

Phase identification was carried out using powder X-ray diffraction (XRD) on a Bruker D8 Advance Diffractometer equipped with a CuK $\alpha$  radiation source, covering a 2 $\theta$  range of 0° to 60°. Lattice parameters were calculated through the least-squares fitting method, employing a minimum of 10 diffraction peaks. The volume fractions of the Bi-2212 and Bi-2201 phases were estimated from the total X-ray intensities (I) of the respective phases using the following equations:

Bi-2212 % = 
$$\frac{\sum I_{2212}}{\sum I_{2212} + \sum I_{2201}} \times 100\%$$
 (1)

and

Bi-2201 % = 
$$\frac{\sum I_{2201}}{\sum I_{2212} + \sum I_{2201}} \times 100\%$$
 (2)

The field emission scanning electron microscopy (FESEM) were obtained using a Merlin Gemini scanning electron microscope. Elemental compositions were determined with an energy dispersive X-ray analyzer (EDX) from Oxford Instruments. Samples were analysed at a magnification of 1000 x and an energy of 15kV.

The electrical resistance measurements of the samples were performed using the four-point probe technique, with silver paste serving as electrical contacts. The experimental setup included a Keithley 197 Autoranging Microvolt DMM and a Keithley 220 Programmable Current Source, operating with a constant current ranging from 1 mA to 100 mA. The distance between the probes was less than 1 mm. A CTI Cryogenics Model 22 closed-cycle helium cryostat and a Lake Shore Model 340 temperature controller were used for cryogenic measurements.

The complex susceptibility ( $\chi = \chi' + i\chi''$ ) was measured using an AC susceptometer (Cryo Industries, model REF-1808-AS) with a frequency of 295 Hz and an applied magnetic field of H = 5 Oe. The critical current density at the peak temperature ( $T_p$ ) of  $\chi''$  was calculated using Bean's model, expressed as  $J_c(T_p) = H/(lw)^{1/2}$  where H is the applied field, and l and w are the dimensions of the bar-shaped sample's cross-sectional area.

#### RESULTS AND DISCUSION

Figure 1 shows the X-ray diffraction patterns where the Bi-2212 phase is dominant over other phases. An impurity phase identified as Bi<sub>2</sub>Sr<sub>2</sub>Cu<sub>1</sub>O<sub>6</sub> (Bi2201) was marked as (\*). The optimum sintering temperature is important to develop the crystallinity of Bi-2212 as shown by sharp and narrow peaks of the XRD patterns [19]. Bi-2212 crystallized at least at 800°C. Furthermore, heating at higher temperatures will develop other phases in the BSCCO system. The first peak 002 at  $2\theta \sim 5.7^{\circ}$ corresponds to the Bi-2212 phase. However, there are small peaks, 020 and 060 which show the presence of Bi-2201 at position  $2\theta \sim 7.2^{\circ}$  and  $\sim 21.7^{\circ}$ respectively. The PDF card used to identify Bi-2212 and Bi-2201 phases are 01-080-2029 and 01-071-5238, respectively. The Bi-2212 peak decreases with MoS<sub>2</sub> addition from 2 to 5 wt.% while Bi-2201 increased accordingly. The volume fraction of the Bi-2201 phase was higher compared to Bi-2212 since the Bi-2201 peaks appeared more. Other than that, the Bi-2212 peaks were observed began to disappear. In this context, MoS<sub>2</sub> addition enhanced the formation of the Bi-2201 phase. MoS<sub>2</sub> peaks are not observed in all samples probably due to the small weight percentage of MoS<sub>2</sub> additions in the Bi-2212 system. In this study, all peaks of Bi-2212 and Bi-2201 phases have been used to estimate the volume fraction [20]. The volume fraction was calculated using the following equations;

$$V_{2212} = \frac{\sum I_{2212}}{\sum I_{2212} + \sum I_{2201} + \sum I_{others}} \times 100\%$$
 (3)

and

$$V_{2201} = \frac{\sum I_{2201}}{\sum I_{2212} + \sum I_{2201} + \sum I_{others}} \times 100\%$$
 (4)

where  $\sum I_{2212}$ ,  $\sum I_{2201}$  and  $\sum I_{others}$  are the sum of intensities of Bi-2212, Bi-2201 phase and other phase, respectively. The volume fraction results are

shown in Table 1. The results indicate a decrease in the volume fraction of the Bi-2212 phase with increasing MoS<sub>2</sub> addition. A higher percentage of the Bi-2212 fraction suggests the development of a single-phase Bi-2212 system. Samples with higher MoS<sub>2</sub> content exhibited an increased volume fraction of the Bi-2201 phase, which correlates with the observed trends in the critical transition temperature. Nearly all diffraction peaks could be

indexed to the orthorhombic lattice structure of Bi-2212. For the x=0 wt.% sample, the lattice parameters were determined to be a=5.367 Å, b=5.410 Å, and c=30.827 Å. In general, no systematic changes were observed in the lattice parameters (a, b, and c) or the unit cell volume across the samples. This suggests that the incorporation of  $MoS_2$  does not significantly disrupt the crystal structure or lattice parameters of the Bi-2212 phase.

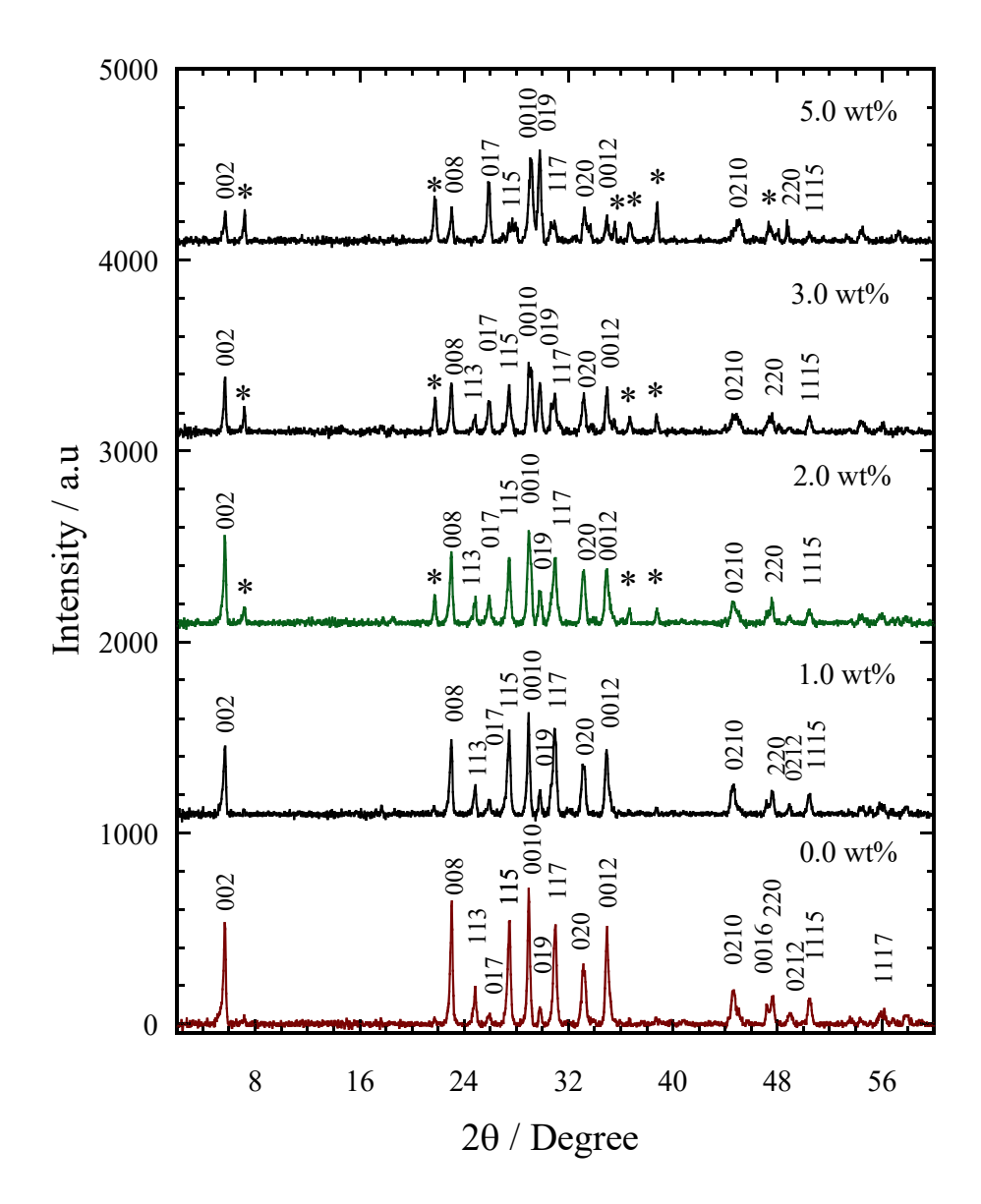


Figure 1. XRD patterns of  $Bi_{1.6}Pb_{0.4}Sr_2CaCu_2O(MoS_2)_x$  for (a) x = 0 - 5 wt.%. Peaks denoted with (\*) indicate Bi-2201.

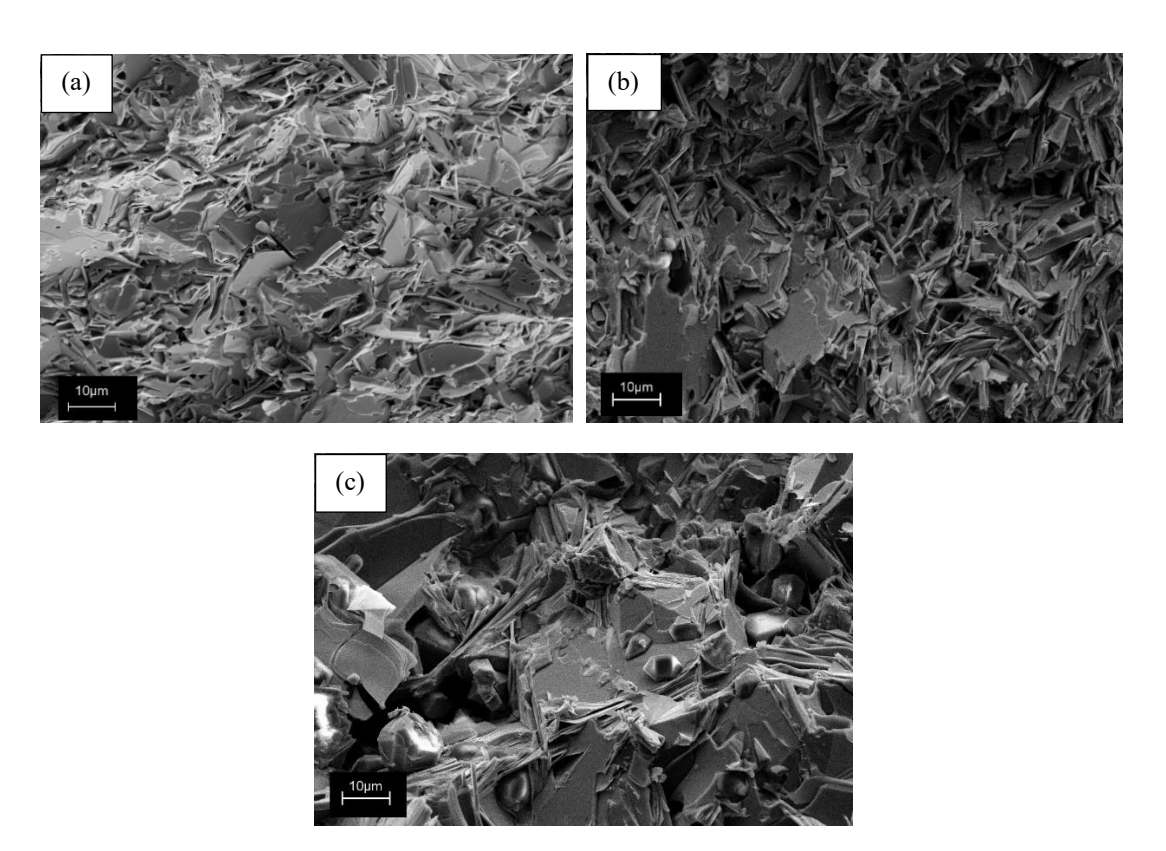


Figure 2. Cross-sectional microstructure of  $Bi_{1.6}Pb_{0.4}Sr_2CaCu_2O_8(MoS_2)_x$  sample for (a) x = 0.0 wt.% (b) x = 2.0 wt.% and (c) x = 5.0 wt.% at magnification of 1000x.

<b>Table 1.</b> $T_{\text{c-ons}}$	set, T <sub>c-zero</sub> , T	$T_{\rm c}$ , $T_{\rm c}\chi$ ,	$T_p$ , $J_c(T_p)$ , $\rho$ , lattice parameters, volume and phase volume	e of
	Bi <sub>1.6</sub>	Pbo 4S	$_{2}$ CaCu <sub>2</sub> O(MoS <sub>2</sub> ), for (a) $x = 0 - 5$ wt.%.	

x	T <sub>c-onset</sub> /K	T <sub>c-zero</sub> /K	Δ <i>T</i> <sub>c</sub> /K	Τ <sub>cχ'</sub> /Κ	<i>T</i> <sub>p</sub> /K	J <sub>c</sub> (T <sub>p</sub> )/A cm <sup>-2</sup>	ρ <sub>297K</sub> /mΩ- cm	a /Å	b /Å	c /Å	V/Å <sup>3</sup>	V <sub>2212</sub> /%	V <sub>2201</sub> /%
0	85	73	12	80	58	31.3	3.72	5.367	5.41	30.827	895.1	>97	<3
1	81	69	12	82	64	24.5	2.34	5.391	5.41	30.852	899.8	>97	<3
2	82	65	17	97	-	20.8	5.98	5.375	5.422	30.885	900.0	90	10
3	83	47	36	94	-	22.1	9.09	5.37	5.422	30.889	899.4	84	16
5	52	-	-	94	-	22.6	46.4	5.279	5.206	30.792	846.2	72	28

The microstructure of Bi-2212 samples, both with and without the addition of MoS<sub>2</sub>, was examined using field emission scanning electron microscopy (FESEM) at a magnification of 1000 x. Three representative samples, with MoS<sub>2</sub> concentrations of x = 0, 2.0, and 5.0 wt.%, were selected to illustrate the microstructural effects. As shown in Figure 2(a-c), all samples exhibited a flaky, plate-like morphology. The sample with x = 2.0wt.% exhibited an average grain size of 1.31 μm, whereas the sample with x = 5.0 wt.% showed a larger average grain size of 1.62 µm. This suggests that the addition of MoS2 particularly at higher concentrations, may influence the alignment and arrangement of the Bi-2212 phase, resulting in larger grain size and reduced flakiness. The increase

in grain size contributed to the suppression of superconducting behaviour.

The variation of resistivity as a function of temperature for all samples is depicted in Figure 3. The figure clearly demonstrates that all samples exhibit metallic behaviour in the normal state, transitioning to superconductivity at lower temperatures. The non-added sample exhibited the highest superconducting transition temperatures, with  $T_{\rm c\ onset}$  at 85 K and  $T_{\rm c\ zero}$  at 73 K. In contrast, samples with MoS<sub>2</sub> addition showed a reduction in  $T_{\rm c\ zero}$ , which may be attributed to Cooper pair breaking. For the sample with x=5 wt.%,  $T_{\rm c\ onset}$  was recorded at 52 K, while  $T_{\rm c\ zero}$  was not observed. The resistance drops in this sample occurred with a broader transition width,

suggesting the presence of the Bi-2201 phase alongside the Bi-2212 phase, likely due to structural phase transformation [21]. These findings are consistent with the volume fraction analysis obtained from XRD. The decrease in  $T_c$  values with increasing MoS<sub>2</sub> content indicates that excess MoS<sub>2</sub> suppresses the superconductivity of the Bi-2212 phase. Higher concentration of MoS<sub>2</sub> led to T<sub>c</sub> suppress since this nanometer-sized MoS<sub>2</sub> may incorporate the lattice structure. Therefore, the optimum charge carrier was modified resulting in T<sub>c</sub> reduction and destroying the superconductivity. Additionally, the room temperature resistivity (p297 K) increased with higher MoS<sub>2</sub> content, as shown in Table 1. Conversely, samples with lower resistivity exhibited higher transition temperatures. Overall, the room temperature resistivity was found to rise with increasing MoS<sub>2</sub> content.

The AC susceptibility versus temperature curves is presented in Figure 4. The transition temperature,  $T_{c\gamma}$  indicates the sudden decrease in the real part of the susceptibility  $\chi$ '. This transition temperature shows that diamagnetic shielding appears, which indicates the onset of the transition temperature of bulk superconductivity. The non-added sample exhibited the highest  $T_{c\chi'}$  (97 K). With the addition of  $MoS_2$ , increased  $T_{c\chi}$ . Two peaks representing the AC losses should be observed in the imaginary part, χ" of susceptibility. Two peaks are typically expected, with a narrower peak at higher temperature representing intrinsic losses (intra-grain coupling) and a broad peak at low temperature due to intergrain coupling losses. However, in this study, there is no sign of intrinsic peaks for all samples. This is attributed to the fact that the applied magnetic field,  $H_{ac} = 5$  Oe is not sufficient for complete penetration of

the Bi-2212 grains. Figure 4 shows  $T_p$  shifts to lower temperatures, indicating that the flux pinning energy in the superconductor is weakened. The addition of smaller amounts of MoS<sub>2</sub> shows improvement of flux pinning since  $T_p$  shifted to a higher temperature compared to the non-added sample. However, an increase in addition to more than x = 1 wt.% suppressed the flux pinning energy. For the non-added sample,  $T_p$  was recorded at 58 K, but no  $T_p$  was observed for samples with x = 2 - 5 wt.% within the measured temperature range of 20 - 100 K. The  $T_p$  curves portray a broad shape with the addition of MoS<sub>2</sub>, showing the weakening of inter-granular coupling. Consistent with previous research [22], adding nanoparticles in amounts exceeding 1 wt.% resulted in a suppression of  $T_c$ , while an improvement in  $T_p$ was observed. In this study,  $T_p$  increased from x = 0 wt.% to x = 1 wt.%. However, with further addition of MoS2, no Tp was detected within the measured temperature range.

The addition of MoS<sub>2</sub> had a more pronounced suppressive effect on the magnetic properties compared to the electrical properties, as evidenced in Table 1. The transport critical current density at the peak temperature,  $J_c(T_p)$ , ranged between 20 and 31 A cm<sup>-2</sup>. Incorporating MoS<sub>2</sub> into the Bi-Sr-Ca-Cu-O system led to a reduction in both the transition temperature and the critical current density. Figure 5 illustrates the relationship between the transition temperature and MoS<sub>2</sub> content, showing a consistent decrease in transition temperature with increasing MoS<sub>2</sub> concentration. In this study, the presence of impurity phases became notably apparent in samples with higher MoS<sub>2</sub> content, a finding that is further supported by the XRD patterns.

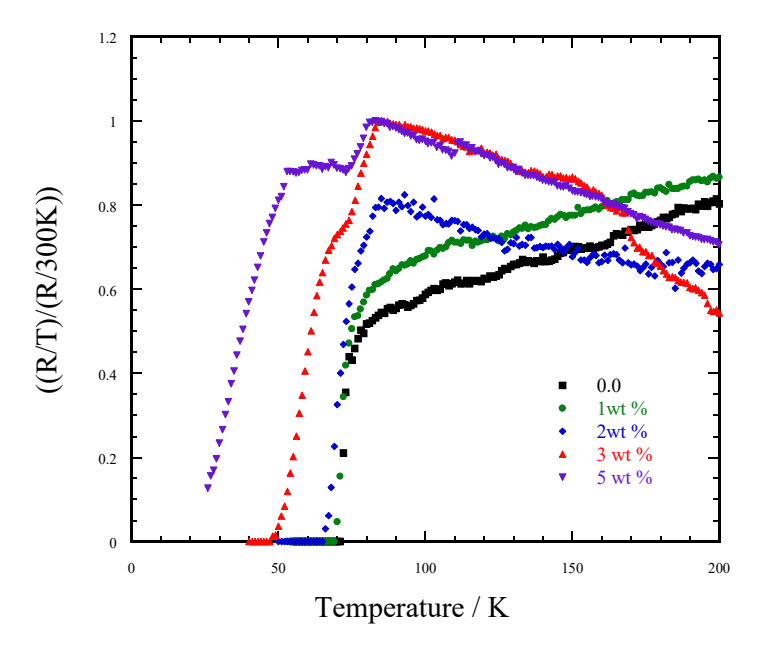
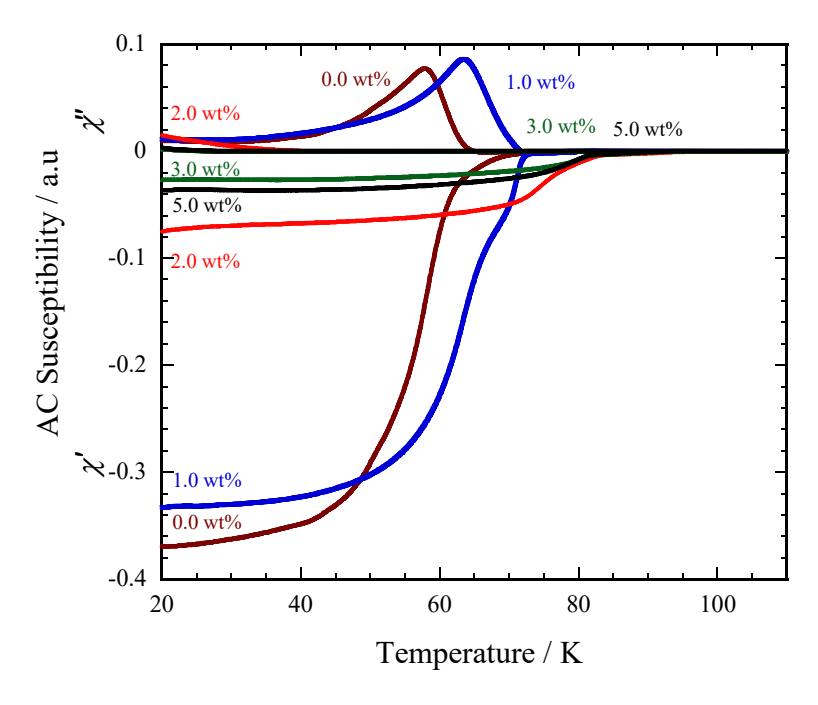
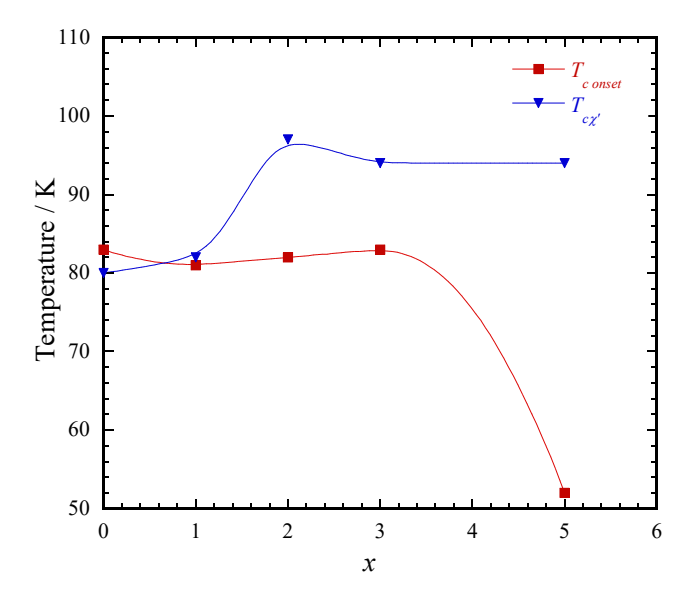


Figure 3. Electrical resistance versus temperature of  $Bi_{1.6}Pb_{0.4}Sr_2CaCu_2O_8(MoS_2)_x$  for x = 0 - 5 wt.%.



**Figure 4.** AC susceptibility  $(\chi = \chi' + i\chi'')$  versus temperature of Bi<sub>1.6</sub>Pb<sub>0.4</sub>Sr<sub>2</sub>CaCu<sub>3</sub>O<sub>8</sub>(MoS<sub>2</sub>)<sub>x</sub> for (a) x = 0 - 5 wt.%.



**Figure 5.**  $T_{\text{c-onset}}$  and  $T_{\text{c}\chi'}$  versus x of  $(\text{Bi}_{1.6}\text{Pb}_{0.4}\text{Sr}_2\text{CaCu}_2\text{O}_8(\text{MoS}_2)_x$  for x = 0 - 5 wt.%.

## CONCLUSION

In conclusion, the effects of  $MoS_2$  on the Bi-Pb-Sr-Ca-Cu-O system were investigated. Increasing the concentration of nanometer-sized  $MoS_2$  addition led to a decrease in both the transition temperature,  $T_c$  and critical current density,  $J_c$ . From the view of microstructure,  $MoS_2$  suppressed the Bi-2212 phase while promoting the Bi-2201 phase. Magnetically, AC susceptibility measurements revealed weakened flux pinning and reduced inter-grain coupling with higher  $MoS_2$  content. These findings suggest that

the controlled incorporation of metal sulfides could provide targeted strategies for modifying grain boundaries and enhancing flux pinning in Bi-2212 superconductors. Further research on metal sulfides could provide valuable insights into their impact on the Bi-2212 superconductor.

### ACKNOWLEDGEMENT

This research was supported by the Ministry of Higher Education, Malaysia under grant no. FRGS/1/2020/STG07/UKM/01/1.

#### REFERENCES

- Fallah-Arani, H., Baghshahi, S., Sedghi, A., Stornaiuolo, D., Tafuri, F., Riahi-Noori, N. (2018) Enhancement in superconducting properties of Bi<sub>2</sub>Sr<sub>2</sub>Ca<sub>1</sub>Cu<sub>2</sub>O<sub>8+θ</sub> (Bi-2212) by means of Boron Oxide additive. *Physica C*, **548**, 31–39.
- Zelati, A., Amirabadizadeh, A., Kompany, A., Salamati, H., Sonier, J. (2014) Effects of Dy<sub>2</sub>O<sub>3</sub> nanoparticle addition on structural and superconducting properties of BSCCO. *Indian Journal of Science and Technology*, 7, 123.
- 3. Hilgenkamp, H. & Mannhart, J. (2002) Grain boundaries in high-Tc superconductors. *Reviews of Modern Physics*, **74(2)**, 485–549.
- Pan, S. H., Hudson, E. W. & Davis, J. C. (2000) STM studies of the electronic structure of vortex cores in Bi<sub>2</sub>Sr<sub>2</sub>CaCu<sub>2</sub>O<sub>8</sub>+δ. *Physical Review Letters*, 85(7), 1536–1539.
- Kaya, C., Özçelik, B., Özkurt, B., Sotelo, A., Madre, M. A. (2012) Effect of Ce substitution on structural and superconducting properties of Bi-2212 system. J. Materi Sci. Mater. Electron, 24, 1580–1586.
- 6. Özkurt, B. (2013) Enhancement in superconducting transition temperature and  $J_c$  values in Na-doped Bi<sub>2</sub>Sr<sub>2</sub>Ca<sub>1</sub>Cu<sub>2-x</sub>Na<sub>x</sub>O<sub>y</sub> superconductors. *J. Mater. Sci. Mater. Electron*, **24**, 2426–2431.
- 7. Hamid, N. and Abd-Shukor, R. (2000) Effects of TiO2 addition on the superconducting properties of Bi-Sr-Ca-Cu-O system. *Journal of Materials Science*, **35(9)**, 2325–2329.
- 8. Miura, A., Oikawa, D., Andoh, H., Sugiura, T., Tsukamoto, T. (2016) Effect of Pr additions to Li-doped Bi2212 bulk superconductors sintered at low temperature. *Phys Procedia*, **81**, 37–40.
- Özkurt, B., Madre, M. A., Sotelo, A., Diez, J. C. (2012) Structural, superconducting, and mechanical properties of Molybdenum substituted Bi<sub>1.8</sub>Sr<sub>2</sub> Ca<sub>1.1</sub>Cu<sub>2.1</sub>O<sub>y</sub>. J. Mater. Sci. Mater. Electron, 24, 1158–1167.
- Zhang, S., Liang, M., Li, C., Hao, Q., Feng, J., Zhang, P. (2015) Enhanced flux pinning properties in Bi-2212 high temperature superconductors with nano-sized precipitates. *MatL*, 157, 197–200.
- Aguiar, J. A., Ramos, A. S., Cabral, L. R., Barbosa, M. V., Awana, V., Ferreira, J., Pavão, A., Chavira, E., Kurmaev, E. (1996) Structural and superconducting properties of MS (M= Fe, Ni or Zn)-substituted. *JPhysCM*, 8, 10545.
- Tyagi, A. K., Sharma, T. (1994) Metallurgical reactions and enhanced magnetic field shielding in YBCO-PbS superconductors. *MatL*, 18, 341–348.

- Amir Zelati, Ahmad Amirabadizadeh, Ahmad Kompany, Hadi Salamati and Jeff Sonier (2014) Effects of Dy<sub>2</sub>O<sub>3</sub> Nanoparticle Addition on Structural and Superconducting Properties of BSCCO. *Indian Journal of Science and Technology*, 7(2), 123–134.
- 14. Aguiar, J. A., Lima, C., Yadava, Y., Tellez, D. L., Ferreira, J., Montarroyos, E. (2000) EDX analysis, microstructure and magnetic properties of CuS doped Bi-2212 superconductors. *Physica C*, **341**, 593–596.
- 15. Farah-Elia, N. A. R., Ilhamsyah, A. B. P., Abd-Shukor R. (2019) Ferrimagnetic Cr<sub>2</sub>S<sub>3</sub> effects on (Bi<sub>1.6</sub>Pb<sub>0.4</sub>) Sr<sub>2</sub>CaCu<sub>2</sub>O<sub>8</sub> superconductor. *J. Mater. Sci. Mater. Electron*, **30**, 12031–12035.
- Loudhaief, N., Ben Salem, M., Labiadh, H., Zouaoui, M. (2020) Electrical properties and fluctuation induced conductivity studies of Bi-based superconductors added by CuS nanoparticles synthesized through the aqueous route. MCP, 242, 122464.
- 17. Dong, Y., Sun, A., Zhang, H., Zhang, M., Xu, B. (2016) The effect of Sn substitution of Pb on microstructure and superconducting properties of Bi–Pb–Sr–Ca–Cu–O superconductor. *Journal of Supercond Nov. Magn.*, **29**, 2765–2769.
- 18. Pearce, C. I., Pattrick, R. A., Vaughan, D. J. (2006) Electrical and magnetic properties of sulphides. *Reviews in Mineralogy and Geochemistry*, **61**, 127–180.
- Darsono, N., Yoon, D. -H., Raju, K. (2016) Effects of the sintering conditions on the structural phase evolution and T<sub>c</sub> of Bi<sub>1.6</sub>Pb<sub>0.4</sub>Sr<sub>2</sub>Ca<sub>2</sub>Cu<sub>3</sub>O<sub>7</sub> prepared using the citrate sol–gel method. *Journal of Supercond Nov. Magn.*, 29, 1491–1497.
- 20. Yavuz, Ş., Bilgili, Ö., Kocabaş, K. (2016) Effects of superconducting parameters of SnO2 nanoparticles addition on (Bi, Pb)-2223 phase. *J. Mater. Sci. Mater. Electron*, **27**, 4526–4533.
- Azhan, J. S. H. H., Azura, C. M. N., Azman, K., Syamsir, S. A. (2016) Structural and electrical properties of high and low Yb doped in Bi2223. *Jurnal Teknologi Science & Engineering*, 78, 6-6, 7–12.
- Aliff-Imran, M. D., Nur-Afrina, M., Masnita, M. J., Hj. Jumali, M. H. and Abd-Shukor, R. (2022) Nano-tin(IV) oxide addition effects on the transport and AC susceptibility parameters of Bi<sub>1.6</sub>Pb<sub>0.4</sub>Sr<sub>2</sub>Ca Cu<sub>2</sub>O<sub>8</sub> superconductor. *Journal of Materials Science: Materials in Electronics*, 33(17), 13947–13955.